5206 *Biochemistry* **2010,** *49,* 5206–5212
DOI: 10.1021/bi100571r

BIOCHEMISTRY
including biophysical chemistry & molecular biology
Article

The 1.4 Å Crystal Structure of the ArsD Arsenic Metallochaperone Provides Insights into Its Interaction with the ArsA ATPase[†]

Jun Ye,[‡,||] A. Abdul Ajees,[§,||] Jianbo Yang,[‡] and Barry P. Rosen*[,§]

[‡]*Department of Biochemistry and Molecular Biology, Wayne State University School of Medicine, Detroit, Michigan 48201, and* [§]*Department of Cellular Biology and Pharmacology, Florida International University, Herbert Wertheim College of Medicine, Miami, Florida 33199*
[||]*These authors contributed equally to this study*

Received April 14, 2010; Revised Manuscript Received May 20, 2010

ABSTRACT: Arsenic is a carcinogen that tops the Superfund list of hazardous chemicals. Bacterial resistance to arsenic is facilitated by ArsD, which delivers As(III) to the ArsA ATPase, the catalytic subunit of the ArsAB pump. Here we report the structure of the arsenic metallochaperone ArsD at 1.4 Å and a model for its binding of metalloid. There are two ArsD molecules in the asymmetric unit. The overall structure of the ArsD monomer has a thioredoxin fold, with a core of four β-strands flanked by four α-helices. Based on data from structural homologues, ArsD was modeled with and without bound As(III). ArsD binds one arsenic per monomer coordinated with the three sulfur atoms of Cys12, Cys13, and Cys18. Using this structural model, an algorithm was used to dock ArsD and ArsA. The resulting docking model provides testable predictions of the contact points of the two proteins and forms the basis for future experiments.

Arsenic places first on the Superfund List of Hazardous Chemicals (http://www.atsdr.cdc.gov/cercla/07list.html) of hazardous substances, in part because it is the most prevalent environmental toxin. The metalloid is a carcinogen and is considered a causative agent of a number of other diseases, including cardiovascular and neurological disorders (*1*, *2*). Both prokaryotes and eukaryotes have arsenic detoxifying systems, frequently involving extrusion from cytosol (*3*).

Various bacterial *ars* operons encode a metallochaperone, ArsD, that transfers As(III) or Sb(III) to the ArsAB ATPase, an efflux pump that extrudes the trivalent metalloids out of cells (*4*, *5*). At present 350 bacterial and 10 archaeal entries for ArsD are present in the NCBI database. The 120-residue ArsD is encoded by the *arsRDABC* operon of plasmid R773 that confers resistance to arsenite and antimonite in *Escherichia coli*. ArsD has three conserved cysteine residues, Cys12, Cys13, and Cys18, that form an As(III) binding site in each subunit of this homodimer (*5*, *6*). ArsD transfers As(III) to the ArsA metalloid binding site formed by cysteine residues 113, 172, and 422 (*7*). How these two proteins interact is not known. The transfer of copper from Atx1-like chaperones to the N-terminal domains of copper efflux pumps involves sequential transfer of metal between cysteine thiolates (*8*). We have proposed a similar sequential transfer mechanism from the cysteine thiolates of ArsD to the cysteine thiolates of ArsA (*9*).

In this study we describe the structure of the R773 apoArsD dimer at 1.4 Å. The ArsD monomer has a thioredoxin fold of four β-strands flanked by four α-helices. Residues 12−22 were mostly disordered, suggesting that the binding site might form when occupied by As(III). The recently deposited coordinates of an oxidized form of an ArsD homologue from *Bacteroides vulgatus* ATCC 8482 (PDB code 3KTB; Y. Kim, C. Tesar, B. Feldmann, and A. Joachimiak, Midwest Center for Structural Genomics, unpublished) allowed modeling of an As(III)-bound form of ArsD. These models suggest how the conformational transition between the apoprotein and metalated ArsD occurs. Finally, the As(III)-bound form of ArsD was docked *in silico* with ArsA at their metalloid binding sites, providing testable predictions for the way in which the two partner proteins interact.

MATERIALS AND METHODS

Expression, Purification, and Crystallization. The last 11 residues of ArsD are not required for metallochaperone activity (*5*), so a truncated form, ArsD109, is routinely used for analysis of interactions with ArsA (*6*). Expression and purification of ArsD109 and its derivatives have been previously reported (*5*, *6*, *9*). However, crystal screens of those proteins produced small, poorly diffracting crystals. To obtain crystals suitable for structural analysis, the DNA sequences corresponding to residues 1−109, along with site-directed mutations C12A, C13A, and C39S, were amplified by PCR and cloned into the pTYB2 expression vector of the IMPACT System (New England BioLabs) as the N-terminal segment fused to the intein and chitin binding domain (CBD)[1] unit, creating chitin binding domain-fused ArsDs (ArsD109-CDB and ArsD109/C12A/C13A/C39S-CDB). Proteins were expressed in *E. coli* strain BL21(DE3)pLysS

[†]This study was supported by National Institutes of Health Grant AI043428.

*To whom correspondence should be addressed. E-mail: brosen@fiu.edu. Tel: (305) 348-0657. Fax: (305) 348-0651.

[1]Abbreviations: CBD, chitin binding domain; SDS, sodium dodecyl sulfate; RMSD, root mean square deviation; Se-Met, selenomethionine; SAD, single-wavelength anomalous dispersion; EXAFS, extended X-ray absorption fine structure; NBD, nucleotide binding domain.

 Published on Web 05/27/2010

Table 1: Data Collection and Refinement Statistics

	SeMet-ArsD	ArsD109	ArsD109/C12A/C13A/C39S
data collection and phasing			
space group	$C2$	$P2_1$	$P2_1$
cell dimensions			
a, b, c (Å)	128.68, 78.18, 37.89	37.68, 74.22, 40.83	37.84, 73.77, 41.25
β (deg)	95.2	97.8	97.3
resolution (Å)	2.3	2.05	1.4
no. of unique reflections	16658 (2428)[a]	13712 (1215)	43232 (6273)
completeness (%)	99.8 (99.5)	97.8 (98.6)	97.9 (97.3)
I/σ	18.0 (6.3)	7.1 (2.2)	16.0 (3.1)
redundancy	7.5 (7.5)	3.12 (3.05)	4.2 (4.2)
R_{sym}	0.101 (0.290)	0.091 (0.348)	0.051 (0.438)
mean figure of merit (before/after density modification)	0.29/0.67		
refinement			
resolution (Å)		40.46−2.05 (2.10−2.05)	40.9−1.4 (1.46−1.4)
I/σ cutoff		0	0
no. of residues		195	190
no. of protein atoms		1526	1492
no. of water molecules		113	268
R/R_{free} (%)		27.1/32.4 (29.7/32.4)	19.2/21.9 (27.7/28.1)
RMSDs			
bonds (Å)		0.028	0.008
angles (deg)		2.3	1.2
bonded B-factors (Å^2), main chain/side chain		1.2/3.5	1.2/3.2

[a]Last shell values are in parentheses.

cells at 37 °C and purified to near homogeneity, and the CBD domain was removed according to the procedure provided with the IMPACT system. To remove minor impurities, proteins were further purified by Superdex 75 chromatography and concentrated to 10 mg/mL. Just prior to crystallization, the buffer was exchanged with 10 mM HEPES, 50 mM NaCl, and 3 mM dithiolthreitol, pH 7.2. The proteins were crystallized at room temperature using the vapor diffusion method with hanging drops consisting of a 1:1 mixture of protein solution and a reservoir solution of 25% PEG 6000, 0.1 M calcium acetate, and 100 mM HEPES, pH 7.4. Prior to data collection, the crystals were flash-frozen in liquid nitrogen with 20% glycerol in the crystallization solution.

Structure Determination, Model Building, and Docking Analysis. Diffraction data were acquired with flash-frozen crystals on the LSCAT-ID32 beamline at the Advanced Photon Source, Argonne, IL. The data were indexed and integrated using MOSFLM (*10*) and scaled and merged using SCALA (*11*). The structure was determined by single-wavelength anomalous dispersion (SAD) (*12*). A data set was collected from a crystal of selenomethionine- (Se-Met-) substituted protein to 2.3 Å resolution. The positions of three of the five Se-Met sites were determined, heavy atom parameters refined, and SAD phases calculated at 2.3 Å resolution using PHENIX (*13*). The Se-Met crystals had three molecules in the asymmetric unit, and an initial model of 261 of the total 330 residues was automatically built with PHENIX. The model was refined in REFMAC (*14*). A data set from a native crystal, an ArsD109 derivative in which Cys12 and Cys13 were replaced by alanine residues (ArsD109/C12A/C13A/C39S), was collected to 1.4 Å resolution. This structure was solved by molecular replacement using the partially refined SAD model. The final model was refined against the 1.4 Å resolution data (97.7% complete) in REFMAC. A native data set from a wild-type crystal was collected on a Rigaku/MSC FR-D rotating-anode X-ray source equipped with an R-AXIS HTC image-plate detector. The wild-type structure was solved by molecular replacement using the refined native structure and refined to 2.05 Å resolution. The COOT Crystallographic Object-Oriented Toolkit available at http://www.biop.ox.ac.uk/coot/ was used for molecular modeling and to superimpose structures. The models were subjected to energy minimization using CHARMM available at http://www.charmm.org/ (*15*). Structural models were rendered using PYMOL (*16*) (http://www.pymol.org) (*16*). ClusPro version 2, a web-based method accessible at http://cluspro.bu.edu/, was used to model ArsD−ArsA interactions. ClusPro is a fully automated docking and discrimination server that filters docked conformations with good surface complementarity and ranks them based on their clustering properties. The server was executed with default parameters.

RESULTS

Model Completeness and Quality. A form of ArsD in which the last 11 residues were replaced by a chitin binding domain (ArsD109-CDB) was constructed for purification purposes. After the intein tag and chitin binding domain were removed, both wild-type and ArsD109/C12A/C13A/C39S proteins crystallized in space group $P2_1$. ArsD109 crystals diffracted to 2.1 Å, and ArsD109/C12A/C13A/C39S diffracted to 1.4 Å. Se-Met ArsD109/C12A/C13A/C39S crystallized in space group $C2$. All three had two molecules in the asymmetric unit (referred to as molecules A and B). The Se-Met data were used to obtain the initial 2.3 Å structure, and 1.4 Å ArsD109/C12A/C13A/C39S diffraction data from the native data set were used to construct the final structure, which was solved by molecular replacement with the Se-Met structure. The structure was refined with final R values of R_{cryst} = 19.2% and R_{free} = 21.9%. The final R_{cryst} and R_{free} values for ArsD109 were 27.1% and 32.4%, respectively, and its structure could be superimposed with the ArsD109/C12A/C13A/C39S structure with an RMS deviation 0.17 Å, so the higher resolution mutant structure was used for subsequent

analysis. Two factors contributed to the relatively high R_{cryst} and R_{free} values: first was a minor twinning problem and high mosaicity (1.5°), and second was the disordered region of the metal binding site. Nevertheless, the electron density map allowed unambiguous fitting of most residues. Molecule A contains residues 1−10 and 24−105; molecule B contains residues 1−11 and 23−109. The remainder, including residues 12, 13, and 18 that form the metalloid binding site in the native protein, are absent from the final model due to lack of interpretable electron density. Analysis of the Ramachandran plots computed using PROCHECK (*17*) shows that 93.1% of the modeled residues are in the most favored regions and no residues in the disallowed region. Data collection and refinement statistics are shown in Table 1. The final coordinates were submitted to the PDB database with access codes 3MWH (ArsD109) and 3KGK (ArsD109/C12A/C13A/C39S).

Overall Structure. There are two ArsD molecules in the asymmetric unit. They form a dimer of approximate 50 × 35 × 30 Å^3 (Figure 1). The two monomers are nearly identical, with a RMSD of 0.52 Å. The termini, especially the C-terminus, are more divergent. The ArsD monomer has a core of four β-strands flanked by four α-helices. Helices α1 and α4 are on one side of the β-strands; α2 and α3 are on the other side. α2 is almost perpendicular to α3, with only one residue between them. β1 is between β2 and β3, parallel to β2 and antiparallel to β3. β3 and β4 form a β-hairpin. Residues 70−72 form a short 3_{10} helix. On molecule B, residues 102−104 also form a short 3_{10} helix.

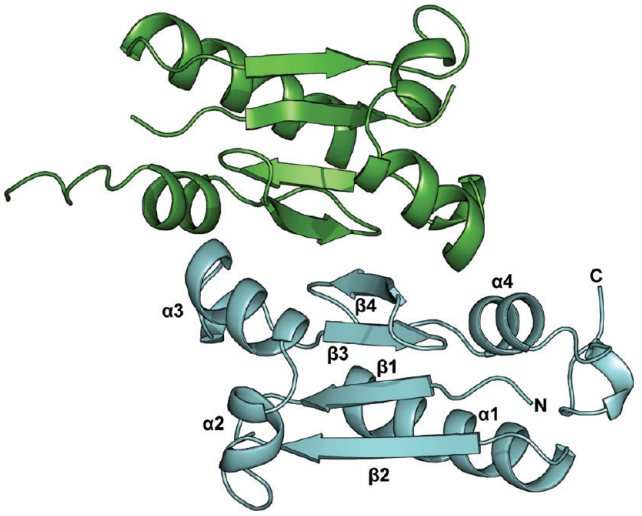

FIGURE 1: ArsD structure. Ribbon diagram of the ArsD109 dimer showing the extensive interface between monomers. Secondary structural units are N-β1-α1-β2-α2-α3-β3-β4-α4-C. Figures were created with PyMOL (*16*).

Monomer−Monomer Interactions. From yeast two-hybrid analysis, ArsD self-associates (*4*), and ArsD purifies as a homodimer (*18*). In the crystallographic dimer, a total surface area of 1380 Å^2 is buried between the two ArsD monomers. This represents 13% of the total solvent-accessible surface, extensive enough to be the interface of the solution form of the ArsD dimer (*19*). Residues of α3, β4, and α4 from both monomers form the interface (Figure 2). The interactions involved in dimerization are primarily hydrophilic. Notably, there are at least 12 hydrogen bonds, and the donors from one monomer and the acceptor from the other are less than 3.2 Å apart. The amide and carbonyl groups of Ala85 from one monomer make hydrogen bonds to the carbonyl and amide of Ala85 from the other monomer, respectively. The hydroxyl of the Ser68 side chain from one monomer is hydrogen bonded to the carbonyl of Val83 from the other monomer. The carbonyl of Gly86 from one monomer also makes hydrogen bonds to the side chain amides of Arg87 from the other monomer. Arg96 and Glu71 form a salt bridge. This extensive network of hydrogen bonds is likely the primary force that holds the monomers together.

Comparison with Thioredoxins. A Dali search (*20*) using the ArsD structure returned thioredoxins as the closest structural homologues of ArsD, with the highest *Z*-score of 6.5 for the *E. coli* thioredoxin TrxA (PDB ID 2TRX) (*21*). The root mean square deviation (RMSD) between the Cα atoms of the 72 aligned residues is 2.5 Å (Supporting Information Figure S1A). TrxA has an N-terminal sequence not present in ArsD, and ArsD α3 is absent in TrxA. The TrxA molecule has a four-residue loop connecting β1 and α1. The TrxA active site sequence $C_{32}PGC_{35}$ is at the beginning of a long α-helix that extends from residue 32 to residue 49, which renders Cys35 solvent inaccessible. Neither of the active site cysteine residues is congruent with Cys12, Cys13, or Cys18 in ArsD. Interestingly, a CACA mutant of TrxA, in which the active site was changed to $C_{32}AC_{34}A$, has the end of the extended helix from residues 35−40 unraveled, exposing Cys34 to solvent, facilitating its participation in catalysis (*22*). In this structure the loop (residues 29−39) is of similar length to the putative loop in ArsD (residues 12−22) (Supporting Information Figure S1B).

Modeling the Metalloid Binding Site. The 2.1 Å structure of a homologue from *B. vulgatus* ATCC 8482 was recently

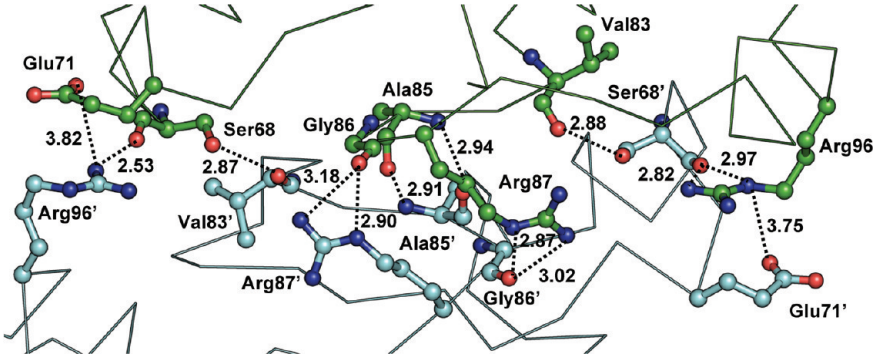

FIGURE 2: The dimer interface. The interface in the crystal structure between the two ArsD monomers (green and cyan) is shown with the backbone atoms in ribbon and the side chains of the interfacial residues in ball and stick. Hydrogen bonds and salt bridges are shown in dotted lines with distances.

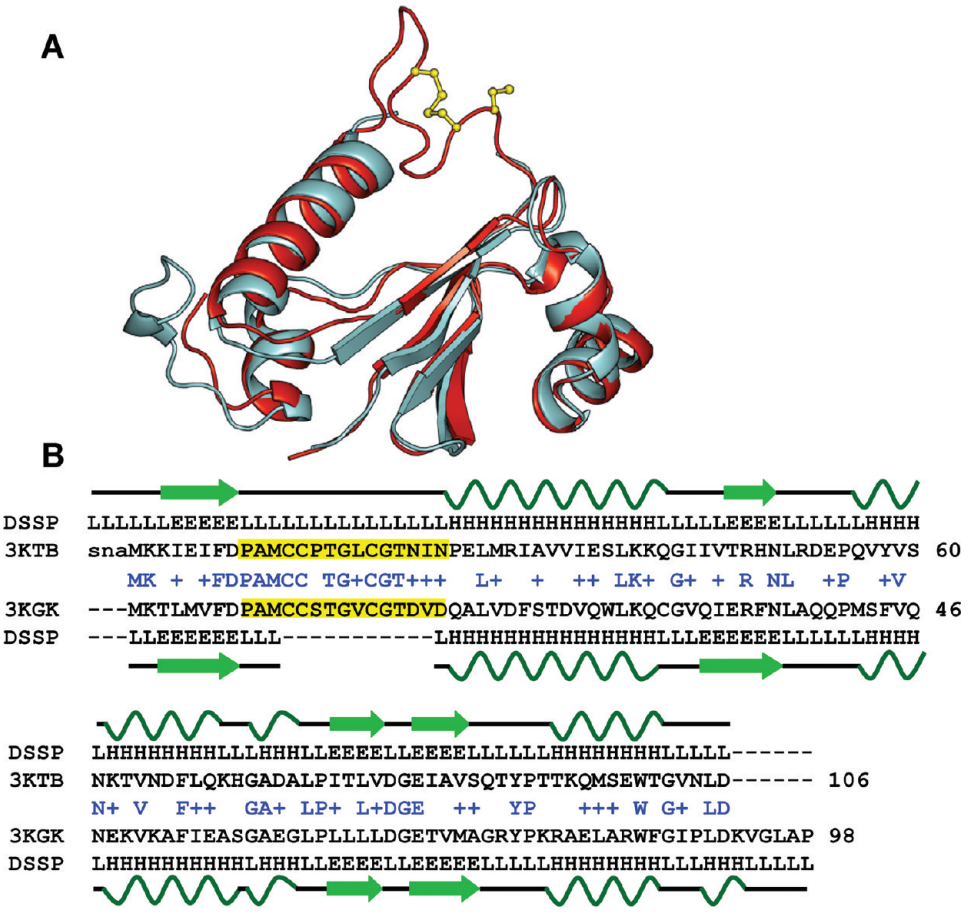

FIGURE 3: Superimposition of the structures of ArsD and 3KTB. (A) The structure of ArsD109 (cyan) was superimposed on the structure of the oxidized form of *B. vulgatus* 3KTB (red). Cys13 and Cys18 (yellow) in 3KTB are disulfide bonded. The 3KTB residue Cys12 (yellow) forms an intersubunit disulfide bond with Cys12 in an adjacent monomer in the unit cell. (B) Structure-based alignment of ArsD and 3KTB. Secondary structural elements are shown in cartoon form (E = strands, L = loops, and H = helices). Residues that form the cysteine-containing loop in 3KTB and the equivalent residues in ArsD109 are highlighted in yellow. Residues that are identical or similar (+) in ArsD and 3KTB are shown in blue.

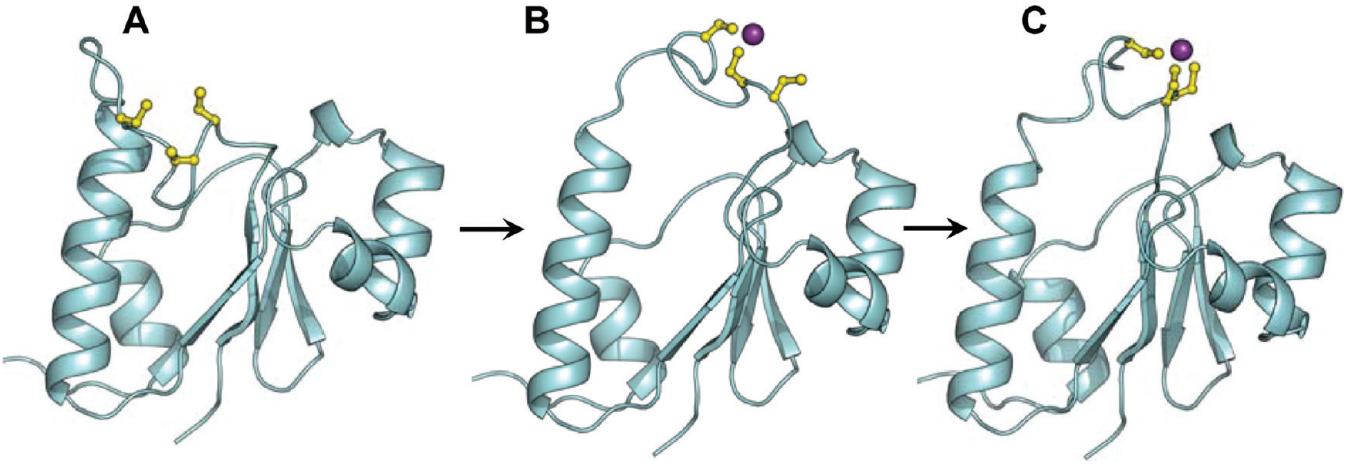

FIGURE 4: The transition from apoArsD to metalated ArsD. Binding of arsenic by apoArsD (A) is proposed to require a minimum of two steps. In the first step, two cysteine thiolates (yellow) bind As(III) (purple sphere) in a transient complex (B). While the order of binding is not known, it is shown here as contributed by Cys13 and Cys18 because those two cysteines form a disulfide bond in the oxidized form of 3KTB. In the second step, the third cysteine thiolate reorients to form the strong three-coordinate binding site (*6*) (C). Residues 11−22 in ArsD109 were modeled on the corresponding residues in 3KTB. The thiolates of the metalloid binding site (yellow) were placed equidistant from the centrally bound arsenic atom (purple sphere) based on the distances determined by EXAFS (*6*).

deposited in the PDB database (PDB code 3KTB; Y. Kim, C. Tesar, B. Feldmann, and A. Joachimiak, Midwest Center for Structural Genomics (MCSG), unpublished). In this structure there are four molecules in the crystallographic unit, as opposed to the dimer form of R773 ArsD109. 3KTB and R773 ArsD109 can be superimposed with an RMSD of 1.0 Å (Figure 3A). In contrast to native ArsD109, where the cysteines are completely reduced, all of the cysteine residues of 3KTB are in intra- and

intermolecular disulfide bonds, likely the result of oxidation during purification. The 11 residues not visible in the R773 ArsD109 structure are contained within a 15-residue loop in *B. vulgatus* ArsD, perhaps because disulfide bond formation rigidified the loop. A structure-based alignment of the two proteins shows that the loops in both are of identical length, and 10 of the 15 loop residues are identical and 4 are similar between the two proteins (Figure 3B). The close homology between the two loops allows the residues not visible in the R773 ArsD109 structure to be modeled with confidence. Based on this information, a model of the metalated form of the R773 ArsD109 (Figure 4) was constructed taking into account the bond distances of 2.24 Å between the sulfur atoms of Cys12, Cys13, and Cys18 and the central arsenic atom determined by EXAFS (*6*) and subjected to energy minimization using CHARMM. We postulate that when the unbound form (Figure 4A) is presented with As(III), it forms an intermediate in which As(III) is weakly bound to Cys13 and Cys18 thiolates (Figure 4B). In the *B. vulgatus* homologue, the Cys12 thiolate is oriented away from other two cysteines, but in the EXAFS structure, all three sulfur atoms become equidistant to the arsenic atom, suggesting that Cys12 could reorient to form the third ligand (Figure 4C). Further experimental results will be necessary to test this proposed order of binding.

Modeling the ArsD−ArsA Interaction. Metalated ArsD interacts with and transfers As(III) to ArsA during catalysis, when the ATPase cycles between open to closed conformations (*5*, *23*). The X-ray crystal structure of ArsA has been solved in the closed form (*24*, *25*). A *Saccharomyces cerevisiae* homologue of ArsA termed Arr4p or Get3 (*26*, *27*) is involved in targeting tail-anchored proteins in the endoplasmic reticulum (*28*). Recently, crystal structures of Get3 from several different yeast were solved in the open (nucleotide free) and closed (ADP-AlF_4^-) conformations (*29*). ArsA has two homologous halves, ArsA1 and ArsA2, each with a nucleotide binding domain (NBD) connected by a short linker, while Get3 is a dimer of two identical monomers, each homologous to either ArsA1 or ArsA2. In the open Get3 conformation there is a large conformational change, and the two monomers are separated by approximately 37° rotation of one subunit toward the other relative to their orientation in the closed form, which is more compact. The ADP-AlF_4^- closed ArsA structure can be superimposed with the Get3 closed structure with an RMSD of 3.4 Å for 420 Cα atoms (Supporting Information Figure S2A). ArsA NBD1 (residue 1−296) and NBD2 (305−583) can be superimposed with the two monomers in the Get3 open structure, with RMSD of 2.3 and 3.0 Å, respectively (Supporting Information Figure S2B). An open model of the ArsA structure based on the open Get3 structure was generated for use for analysis of ArsA−ArsD interactions and docking studies (Figure 5).

Views of the open form of ArsA from opposite directions (Figure 5) display a cavity into which ArsD can fit. To examine whether the structures have complementary surfaces, the open ArsA and metalated ArsD models were docked by using the fully automated, web-based program ClusPro version 2.0 with default parameters. The ClusPro docking server yielded 108 top-scoring solutions based on the balanced, electrostatic-favored, hydrophobic-favored, van der Waals plus electrostatic-favored coefficients. Since biochemical analysis indicates that the three cysteines of ArsD and the three cysteines of ArsA must be in proximity for transfer (*5*), the 77 solutions that did not meet this constraint were discarded. Most of those had ArsD binding based on hydophobic-favored and van der Waals-favored coefficients to various locations on the surface of ArsA. This left 31 solutions in which ArsD fit into the cavity formed between the two halves of ArsA. Of these, the one most consistent with the demonstrated proximity of the cysteine residues of ArsD and ArsA (*4*) had ArsD sulfur atoms of Cys12 and Cys13 within 4.1−7.5 Å of the sulfur atoms of ArsA residues Cys113 and Cys172 (Figure 6).

DISCUSSION

A number of copper, iron, and nickel metallochaperones have been identified (*30*), and several have been characterized at the molecular level (*8*, *31*), but ArsD is the only identified arsenic metallochaperone. Like the yeast copper chaperone Atx1p, which binds and transfers intracellular copper to the copper efflux pump Ccc2p (*8*), ArsD binds and transfers intracellular arsenic to the arsenic ArsAB efflux pump (*4*). The interaction of the copper chaperone CCS in complex with its partner protein, superoxide dismutase, has been elucidated crystallographically (*32*). While transfer of copper from Atx1p to Ccc2p has not been examined at that level, their interaction has been explored by *in silico* docking (*33*).

In this study a combination of X-ray crystallography and *in silico* modeling and docking was used to examine the structure of ArsD and its interaction with the partner protein, ArsA. To explore the interactions of ArsD and ArsA requires a structural description of the form of ArsA to which ArsD transfers As(III). ArsA undergoes a number of conformational transitions during the catalytic cycle, an open form in the absence of ATP and As(III), and a closed form when both are present (*7*, *34*). We have reported the structure of the closed form with different nucleotides and metalloids (*25*, *35*). However, since metalloid transfer requires ArsA to be undergoing catalysis (*6*), it is likely that ArsD initially interacts with an open form of ArsA. During As(III) transfer from ArsD, ArsA undergoes a number of conformational changes, so the model shown in Figure 6 generated by *in silico* docking of metalated ArsD with an open form of ArsA may reflect only an initial intermediate in the transfer process but provides insights into the contact regions of the two proteins. The docked proteins are shown in two different orientations that differ by 90° in Figure 6A (ribbon) and Figure 6B (surface) to illustrate the reasonableness of the fit. Not only does ArsD fit well into the cavity of the open form of ArsA but the residues of the two proteins that are proposed to interact exhibit reasonable complementarity. Proposed ArsD residues that interact with ArsA are labeled in Figure 6C. Residues that interact with ArsA1 are to the left of the dotted line, and to the right are those that interact with ArsA2. ArsA residues proposed to interact with ArsD are labeled in Figure 6D, with ArsA1 colored green and ArsA2 colored orange. Overall, 30 ArsD residues are predicted to be within 4 Å of 20 residues of ArsA (Table 2). Many of these ArsD residues are positively charged (e.g, Lys2, Arg45, and Arg87) or negatively charged (e.g., Asp21, Asp23, Glu66, and Asp71). These residues are each close enough to form charge pairs with residues in ArsA. For example, ArsD residues Arg45 and Arg87 are close enough to ArsA residues Asp417 and Glu168, respectively, to form charge pairs. These and other predictions from modeling will be tested by mutagenesis in future analyses.

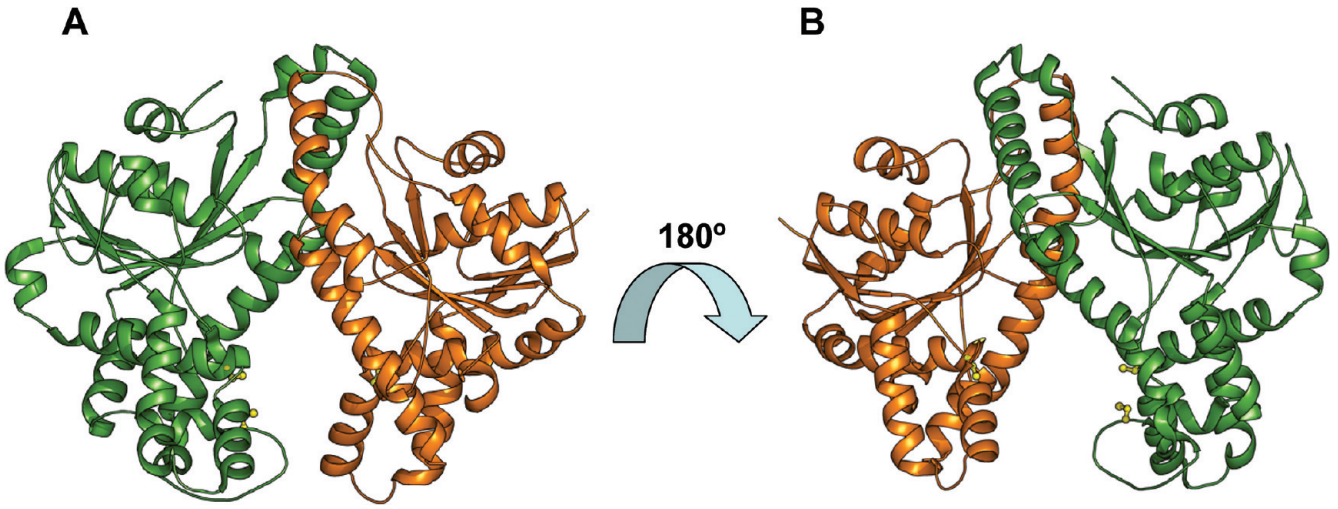

FIGURE 5: An ArsA open model. The open (nucleotide free) form of ArsA was modeled on the open form of *Schizosaccharomyces pombe* Get3 (Supporting Information Figure S2B). The three cysteines residues of ArsA that form the As(III) binding site (*24*, *25*) are shown in yellow. The structure is shown in two orientations (A and B) that differ by 180° to illustrate the cavity between ArsA1 and ArsA1 into which ArsD is proposed to fit.

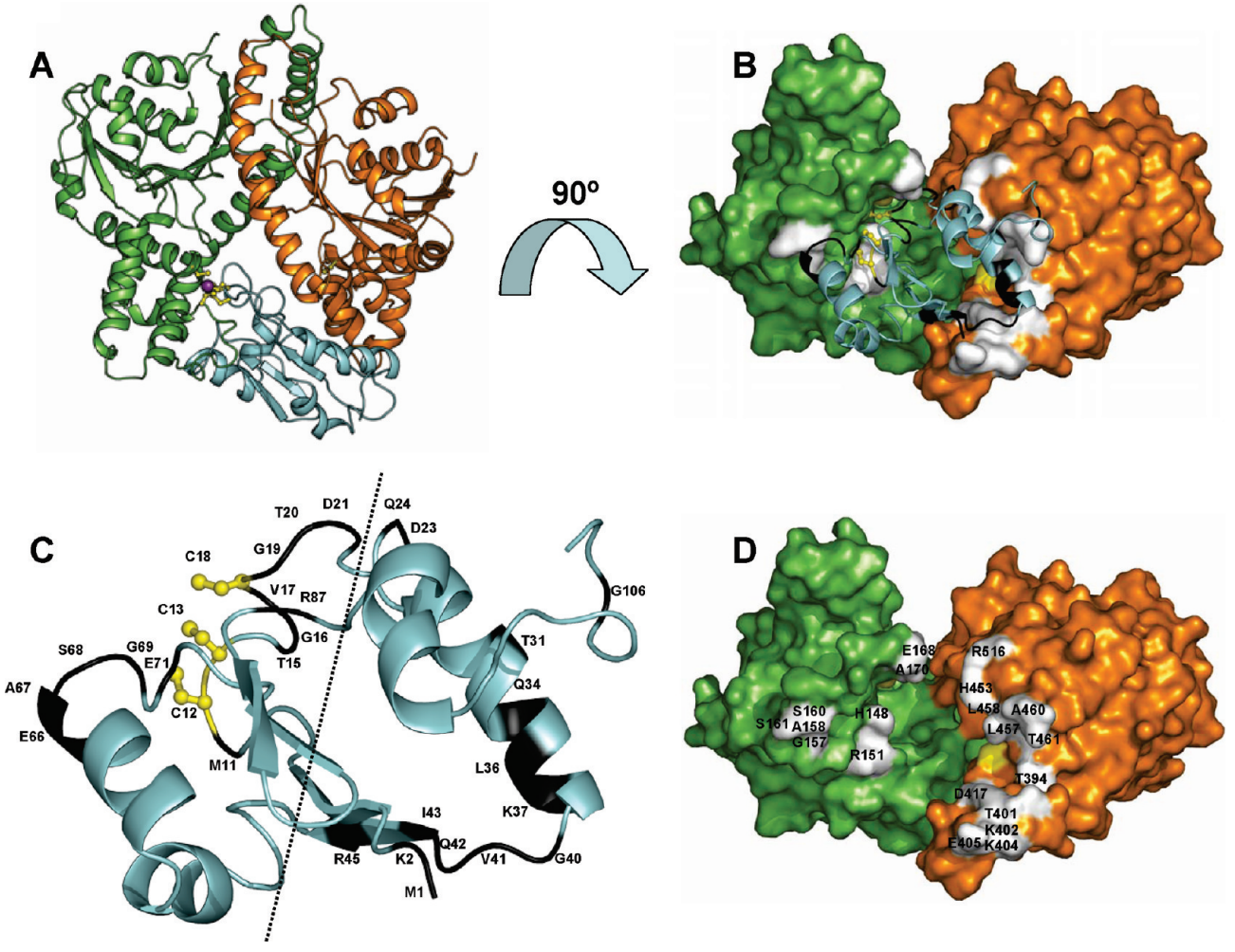

FIGURE 6: Modeling the ArsD−ArsA complex. (A) An optimized model based on *in silico* docking analyses is shown in the ribbon diagram. ArsD (cyan) is proposed to fit into the cavity of the open form of ArsA (ArsA1 in green and ArsA2 in orange). The arsenic atom (purple sphere) is bound to the thiolates (yellow ball and sticks) of ArsD residues 12, 13, and 18, which are within 4 Å of the sulfur atoms of ArsA1 residues Cys113 and Cys172. In a subsequent putative step Cys422 of ArsA2 would reorient to form the third ArsA ligand to As(III). (B) The ArsD−ArsA complex is shown vertically rotated 90°, with a surface rendering of ArsA, revealing ArsD residues (black) that are predicted to interact with ArsA residues (white). (C) ArsD is shown alone in the same orientation as in (B). Residues predicted to interact with ArsA are labeled. Residues on the left side of the dotted line are proposed to interact with residues in ArsA1 and those on the right side of the dotted line with ArsA2. (D) ArsA is shown alone in the same orientation as in (B). The labeled residues in white are predicted to interact with ArsD.

Table 2: ArsA and ArsD Residues Predicted from *in Silico* Docking To Be within 4 Å of Each Other

ArsA residues	ArsD residues
His148	Cys13, Thr15, Gly16, Val17, Cys18
Arg151	Met11, Cys12
Gly157	Glu71
Ala158	Glu71
Ser160	Glu66, Ala67
Ser161	Ala67, Ser68, Gly69
Glu168	Arg87
Ala170	Gly19, Thr20
Tyr394	Lys37
Thr401	Leu36, Lys37, Gly40, Val41
Lys402	Lys37, Val41, Ile43
Lys404	Gln42
Glu405	Met1, Lys2, Gln42
Asp417	Arg45
His453	Asp21, Asp23
Leu457	Gln34
Leu458	Gln34
Ala460	Thr31
Thr461	Gln34, Gly106
Arg516	Asp21, Asp23, Gln24

SUPPORTING INFORMATION AVAILABLE

Additional figures as described in the text. This material is available free of charge via the Internet at http://pubs.acs.org.

REFERENCES

1. Abernathy, C. O., Thomas, D. J., and Calderon, R. L. (2003) Health effects and risk assessment of arsenic. *J. Nutr. 133*, 1536S–1538S.
2. Beane Freeman, L. E., Dennis, L. K., Lynch, C. F., Thorne, P. S., and Just, C. L. (2004) Toenail arsenic content and cutaneous melanoma in Iowa. *Am. J. Epidemiol. 160*, 679–687.
3. Bhattacharjee, H., and Rosen, B. P. (2007) Arsenic metabolism in prokaryotic and eukaryotic microbes, in Molecular microbiology of heavy metals (Nies, D. H. S., and Simon, Eds.) pp 371−406, Springer-Verlag, Heidelberg/New York.
4. Lin, Y. F., Walmsley, A. R., and Rosen, B. P. (2006) An arsenic metallochaperone for an arsenic detoxification pump. *Proc. Natl. Acad. Sci. U.S.A. 103*, 15617–15622.
5. Lin, Y. F., Yang, J., and Rosen, B. P. (2007) ArsD residues Cys12, Cys13, and Cys18 form an As(III)-binding site required for arsenic metallochaperone activity. *J. Biol. Chem. 282*, 16783–16791.
6. Yang, J., Rawat, S., Stemmler, T. L., and Rosen, B. P. (2010) Arsenic binding and transfer by the ArsD As(III) metallochaperone. *Biochemistry 49*, 3658−3666.
7. Ruan, X., Bhattacharjee, H., and Rosen, B. P. (2008) Characterization of the metalloactivation domain of an arsenite/antimonite resistance pump. *Mol. Microbiol. 67*, 392–402.
8. Boal, A. K., and Rosenzweig, A. C. (2009) Structural biology of copper trafficking. *Chem. Rev. 109*, 4760–4779.
9. Lin, Y. F., Yang, J., and Rosen, B. P. (2007) ArsD: an As(III) metallochaperone for the ArsAB As(III)-translocating ATPase. *J. Bioenerg. Biomembr. 39*, 453–458.
10. Powell, H. R. (1999) The Rossmann Fourier autoindexing algorithm in MOSFLM. *Acta Crystallogr., Sect. D: Biol. Crystallogr. 55*, 1690–1695.
11. Evans, P. (2006) Scaling and assessment of data quality. *Acta Crystallogr., Sect. D: Biol. Crystallogr. 62*, 72–82.
12. Ealick, S. E. (2000) Advances in multiple wavelength anomalous diffraction crystallography. *Curr. Opin. Chem. Biol. 4*, 495–499.
13. Adams, P. D., Gopal, K., Grosse-Kunstleve, R. W., Hung, L. W., Ioerger, T. R., McCoy, A. J., Moriarty, N. W., Pai, R. K., Read, R. J., Romo, T. D., Sacchettini, J. C., Sauter, N. K., Storoni, L. C., and Terwilliger, T. C. (2004) Recent developments in the PHENIX software for automated crystallographic structure determination. *J. Synchrotron Radiat. 11*, 53–55.
14. Winn, M. D., Murshudov, G. N., and Papiz, M. Z. (2003) Macromolecular TLS refinement in REFMAC at moderate resolutions. *Methods Enzymol. 374*, 300–321.
15. Brooks, B. R., Brooks, C. L., III, Mackerell, A. D., Jr., Nilsson, L., Petrella, R. J., Roux, B., Won, Y., Archontis, G., Bartels, C., Boresch, S., Caflisch, A., Caves, L., Cui, Q., Dinner, A. R., Feig, M., Fischer, S., Gao, J., Hodoscek, M., Im, W., Kuczera, K., Lazaridis, T., Ma, J., Ovchinnikov, V., Paci, E., Pastor, R. W., Post, C. B., Pu, J. Z., Schaefer, M., Tidor, B., Venable, R. M., Woodcock, H. L., Wu, X., Yang, W., York, D. M., and Karplus, M. (2009) CHARMM: the biomolecular simulation program. *J. Comput. Chem. 30*, 1545–1614.
16. DeLano, W. L. (2001) The PyMOL user's manual, DeLano Scientific, San Carlos, CA.
17. Laskowski, R. A., Rullmannn, J. A., MacArthur, M. W., Kaptein, R., and Thornton, J. M. (1996) AQUA and PROCHECK-NMR: programs for checking the quality of protein structures solved by NMR. *J. Biomol. NMR 8*, 477–486.
18. Chen, Y., and Rosen, B. P. (1997) Metalloregulatory properties of the ArsD repressor. *J. Biol. Chem. 272*, 14257–14262.
19. Kobe, B., Guncar, G., Buchholz, R., Huber, T., Maco, B., Cowieson, N., Martin, J. L., Marfori, M., and Forwood, J. K. (2008) Crystallography and protein-protein interactions: biological interfaces and crystal contacts. *Biochem. Soc. Trans. 36*, 1438–1441.
20. Holm, L., Kaariainen, S., Rosenstrom, P., and Schenkel, A. (2008) Searching protein structure databases with DaliLite v.3. *Bioinformatics 24*, 2780–2781.
21. Katti, S. K., LeMaster, D. M., and Eklund, H. (1990) Crystal structure of thioredoxin from *Escherichia coli* at 1.68 Å resolution. *J. Mol. Biol. 212*, 167–184.
22. Collet, J. F., Peisach, D., Bardwell, J. C., and Xu, Z. (2005) The crystal structure of TrxA(CACA): insights into the formation of a [2Fe-2S] iron-sulfur cluster in an *Escherichia coli* thioredoxin mutant. *Protein Sci. 14*, 1863–1869.
23. Ruan, X., Bhattacharjee, H., and Rosen, B. P. (2006) Cys-113 and Cys-422 form a high affinity metalloid binding site in the ArsA ATPase. *J. Biol. Chem. 281*, 9925–9934.
24. Zhou, T., Radaev, S., Rosen, B. P., and Gatti, D. L. (2000) Structure of the ArsA ATPase: the catalytic subunit of a heavy metal resistance pump. *EMBO J. 19*, 1–8.
25. Zhou, T., Radaev, S., Rosen, B. P., and Gatti, D. L. (2001) Conformational changes in four regions of the *Escherichia coli* ArsA ATPase link ATP hydrolysis to ion translocation. *J. Biol. Chem. 276*, 30414–30422.
26. Shen, J., Hsu, C. M., Kang, B. K., Rosen, B. P., and Bhattacharjee, H. (2003) The *Saccharomyces cerevisiae* Arr4p is involved in metal and heat tolerance. *Biometals 16*, 369–378.
27. Auld, K. L., Hitchcock, A. L., Doherty, H. K., Frietze, S., Huang, L. S., and Silver, P. A. (2006) The conserved ATPase Get3/Arr4 modulates the activity of membrane-associated proteins in *Saccharomyces cerevisiae*. *Genetics 174*, 215–227.
28. Bozkurt, G., Stjepanovic, G., Vilardi, F., Amlacher, S., Wild, K., Bange, G., Favaloro, V., Rippe, K., Hurt, E., Dobberstein, B., and Sinning, I. (2009) Structural insights into tail-anchored protein binding and membrane insertion by Get3. *Proc. Natl. Acad. Sci. U.S.A. 106*, 21131–21136.
29. Mateja, A., Szlachcic, A., Downing, M. E., Dobosz, M., Mariappan, M., Hegde, R. S., and Keenan, R. J. (2009) The structural basis of tail-anchored membrane protein recognition by Get3. *Nature 461*, 361–366.
30. Rosenzweig, A. C. (2002) Metallochaperones: bind and deliver. *Chem. Biol. 9*, 673–677.
31. Bencze, K. Z., Kondapalli, K. C., Cook, J. D., McMahon, S., Millan-Pacheco, C., Pastor, N., and Stemmler, T. L. (2006) The structure and function of frataxin. *Crit. Rev. Biochem. Mol. Biol. 41*, 269–291.
32. Lamb, A. L., Torres, A. S., O'Halloran, T. V., and Rosenzweig, A. C. (2001) Heterodimeric structure of superoxide dismutase in complex with its metallochaperone. *Nat. Struct. Biol. 8*, 751–755.
33. Arnesano, F., Banci, L., Bertini, I., and Bonvin, A. M. (2004) A docking approach to the study of copper trafficking proteins; interaction between metallochaperones and soluble domains of copper ATPases. *Structure 12*, 669–676.
34. Zhou, T., and Rosen, B. P. (1997) Tryptophan fluorescence reports nucleotide-induced conformational changes in a domain of the ArsA ATPase. *J. Biol. Chem. 272*, 19731–19737.
35. Zhou, T., Rosen, B. P., and Gatti, D. L. (1999) Crystallization and preliminary X-ray analysis of the catalytic subunit of the ATP-dependent arsenite pump encoded by the *Escherichia coli* plasmid R773. *Acta Crystallogr., Sect. D: Biol. Crystallogr. 55*, 921–924.